

Charged Scalar Field at Future Null Infinity via Nonlinear Hyperboloidal Evolution

João D. Álvares ^{1,2,*} and Alex Vaño-Viñuales ^{1,3,†}

¹*CENTRA, Departamento de Física do Instituto Superior Técnico (IST),
Universidade de Lisboa, 1049-001 Lisboa, Portugal*

²*Instituto de Telecomunicações (IT), Universidade de Aveiro Campus Universitário de Rua Santiago, 3810-193 Aveiro*

³*Departament de Física, Universitat de les Illes Balears,
IAC3, Carretera Valldemossa km 7.5, E-07122 Palma, Spain*

Quasinormal modes and power-law late-time decay tails of a charged scalar field in a charged black hole background have been studied, but never in the fully non-linear regime, as far as we know. In this paper, we study the dependence of these properties on the charges of scalar field and black hole. For the quasinormal modes, a fit of the spherical fundamental mode is shown for the purely uncharged case and compared to the charged one. We also see for the first time the transition from gravitational decay to pure electromagnetic decay, and show disagreement with the oscillation frequency between real and imaginary parts of the scalar field prescribed in the literature. Full non-linear evolutions of hyperboloidal slices in spherical symmetry were used to obtain our results, allowing for the extraction of signals at future null infinity.

I. INTRODUCTION

Valuable information about compact objects and their induced spacetime deformations can be retrieved by studying the behaviour of the system after dynamical perturbations. In general relativity, such relaxation takes the form of quasi-normal mode (QNM) ringing [1–4], followed by power-law decay tails [5–7]. Both propagate across the whole spacetime until infinity, where they are unambiguously characterized. These effects are variations around a stationary state achieved in the long term, which makes perturbation theory a suitable tool to gain insights into them. A very relevant question concerns the regime of validity of the description by the linear theory. Taking as example the ringdown of a coalescence of compact objects, when after the non-linear merger is the perturbative approach an appropriate description? Only through comparisons between the full non-linear case and linear approximations can the faithfulness of the latter be judged. In this work in spherical symmetry we numerically evolve scalar perturbations of the Reissner-Nortström (RN) spacetime using the coupled general relativity, Maxwell and complex massless Klein-Gordon systems in the full non-perturbative regime reaching null infinity and compare them to prior estimates in the literature.

The seminal work [5] motivated a still-growing interest in QNMs and power-law decay tails. For the case of a real scalar field, the power-law decay comes from the backscattering of outgoing waves of the scalar field at late-times, due to the effective potential created by the presence of a black hole. Being l the mode of the scalar field ϕ , in the limit of timelike infinity the expectation is

that

$$\phi \propto t^{-2l-2}. \quad (1)$$

Shortly afterwards, Ref. [8] extended the late-time power-laws to the charged scalar field collapsing into a RN black hole. The same power-law as (1) was predicted, but with the signal dominated by slower decaying primary waves.

About two decades later, Ref. [6] studied massless scalar field perturbations in fixed Schwarzschild and RN spacetimes, but this time also focusing on future null infinity – the collection of the end-points of future-directed null geodesics. Not long after, Hod and Piran¹ published a three-paper investigation on the late-time evolution of charged gravitational collapse and decay of charged scalar hair [9–11]. In Ref. [9] they agreed with Ref. [8], but only for the regime of $qQ \ll 1$, where q is the scalar field's charge parameter and Q is the black hole's charge. The second paper then corrects the expected power-law for general values of qQ , reading

$$\phi \propto t^{-2\beta+2} \quad (2)$$

at timelike infinity. The quantity β is defined as,

$$\beta = \frac{-1 + \sqrt{(2l+1)^2 - 4(qQ)^2}}{2}. \quad (3)$$

At future null infinity, they also predict that,

$$\phi \propto u^{-(\beta+1-iqQ)}, \quad (4)$$

where u denotes the retarded time. The difference between (1) and (3) is that as the parameter qQ increases, the electromagnetic coupling between the charged scalar

*Electronic address: joaodinis01@tecnico.ulisboa.pt

†Electronic address: alex.vano@uib.es

¹ We mention the authors' names for ease of comparison with their results in Figs. 7 and 8.

field's real and imaginary parts becomes stronger and the QNMs that we expect to see start to be dominated by electromagnetism. The same goes for the tail decay.

More recently, Ref. [12] generalized for the massive charged scalar field in the Kerr-Newman background, but their analysis for the massless charged scalar field is inconclusive. Although the RN spacetime, which we consider here, does not include the presence of angular momentum, it can be used as a toy-model of the Kerr or Kerr-Newman black holes, as it includes the possibility of extremal behaviour when its charge Q equals its mass M .

The late-decay of the power-law tails can be evaluated along a timelike curve asymptoting to future timelike infinity i^+ and along future null infinity \mathcal{I}^+ . The former is out of reach for traditional numerical simulations, where the system would need to be evolved forever to reach it. Exceptions are implementations that use a compactification in the time coordinate such as Ref. [13]. Still, evolving for a long time in a typical implementation allows to see the decay along a timelike curve. Observing the decay along future null infinity however requires a different construction. The following options allow to reach it numerically: evolution on single or double null slices [14], Cauchy-characteristic extraction/evolution [15–17], Cauchy-characteristic matching [18–20] and hyperboloidal evolution [21–24]. The approach taken in this work is free evolution of the Einstein equations using the BSSN/Z4 formalism [25–28] via conformal compactification [21] on hyperboloidal slices [29]. Previous work on this research line is given by the series [30–35] where the Einstein and Klein-Gordon equations were evolved on hyperboloidal slices in spherical symmetry. Recently, Ref. [36] extended this to include the Maxwell equations, showing the capability of the formalism to simulate electrically charged spacetimes.

In this paper we present evolutions of a charged scalar field with a charged black hole at the center of the spacetime, going from the purely neutral case ($Q = 0$) to the extremal one ($M = Q$) [37]. Since we will be working in spherical symmetry, we will only consider the modes with $l = 0$. Given the efficiency of extracting radiation at future null infinity when using hyperboloidal slices, it is easy to check late-time behavior for several values of qQ . This will be important to understand the transition of the scalar field's late-time properties from gravitationally-led effects to electromagnetically-led effects.

The paper is organized as follows: the Einstein-Maxwell-Klein-Gordon system as implemented in [36] is briefly described in section II, followed up by the initial data for the simulations in section III. The QNM analysis is done in section IV and the tail regime is discussed in section V and VI. For convergence tests of the implementation we redirect the reader to Ref. [36]. The conclusions are presented in section VII.

II. SYSTEM SETUP

A detailed presentation of the setup is given in Ref. [36]. Here we provide a brief summary. The system to be considered is described by the following action [38, 39],

$$S = \int (R - 8\pi[(\mathcal{D}_\mu\phi)^*(\mathcal{D}^\mu\phi)] - F^{\mu\nu}F_{\mu\nu})\sqrt{-g}d^4x, \quad (5)$$

where R is the Ricci scalar, $\mathcal{D}_\mu = \nabla_\mu + iqA_\mu$ is the gauge invariant covariant derivative, $F_{\mu\nu}$ is the Faraday/electromagnetic tensor, and ϕ is the charged complex scalar field, as mentioned before. The equations of motion that rule our system are the Einstein equations, the massless Klein-Gordon equation and Maxwell's equations, given by

$$\begin{aligned} G_{\mu\nu} &= 8\pi T_{\mu\nu}, \\ \mathcal{D}_\mu\mathcal{D}^\mu\phi &= 0, \\ \nabla^\mu F_{\mu\nu} &= 4\pi J_\nu, \end{aligned} \quad (6)$$

with

$$J_\mu = \frac{iq}{2}[\phi^*\mathcal{D}_\mu\phi - \phi(\mathcal{D}_\mu\phi)^*], \quad (7)$$

where the asterisk means the complex conjugate. The Einstein field equations will be evolved using the BSSN/conformal Z4 formalism [25–28] following the approach in [31, 36]. Contrary to [5, 6, 8–12], where the backreaction of the stress-energy tensor on the spacetime is neglected and thus the background spacetime is not evolved, here we consider the fully coupled case. The stress-energy tensor of this system reads

$$\begin{aligned} T_{\mu\nu} &= F_{\mu\alpha}F_\nu^\alpha - \frac{1}{4}g_{\mu\nu}F_{\alpha\beta}F^{\alpha\beta} \\ &+ \mathcal{D}_\mu\phi\mathcal{D}^\nu\phi - \frac{1}{2}g_{\mu\nu}\mathcal{D}^\alpha\phi\mathcal{D}_\alpha\phi. \end{aligned} \quad (8)$$

We will be assuming spherical symmetry, so of the electric and magnetic fields that the Faraday tensor is usually decomposed into, we will discard the magnetic field and evolve the electric one. See Ref. [36] for more details of the setup.

A. Hyperboloidal Slices and Conformal Compactification

To be able to extract radiation at \mathcal{I}^+ , we will use hyperboloidal slices, given by the level sets of a new time variable t related to the physical \tilde{t} as

$$t = \tilde{t} - h(\tilde{r}), \quad (9)$$

where $h(\tilde{r})$ is the height function, whose effect is to raise the slices so they reach \mathcal{I}^+ . We also introduce a compactification factor, $\tilde{\Omega}$, such that

$$\tilde{r} = \frac{r}{\tilde{\Omega}(r)}. \quad (10)$$

Its purpose is to map the position of \mathcal{S}^+ to a given finite radius $r_{\mathcal{S}^+}$. Finally we do a conformal compactification, such that the components of the rescaled metric $\bar{g}_{\mu\nu}$ do not diverge at \mathcal{S}^+ ,

$$\bar{g}_{\mu\nu} = \Omega^2 \tilde{g}_{\mu\nu}. \quad (11)$$

The conformal factor Ω is chosen to be

$$\Omega = -K_{\text{CMC}} \frac{r_{\mathcal{S}^+}^2 - r^2}{6r_{\mathcal{S}^+}}, \quad (12)$$

where K_{CMC} is a (negative) constant. Initially it coincides with the trace of the physical extrinsic curvature, providing constant-mean-curvature slices.

B. Einstein Field Equations Formulation

From now on, variables with a tilde on top will refer to the physical quantities, while those with a bar or nothing on top will correspond to conformally rescaled ones. Applying the 3+1 decomposition to the conformally compactified metric, we define the spatial part of the metric $\tilde{\gamma}_{ij}$. In the BSSN formalism it is decomposed into a spatial conformal factor χ and a conformally rescaled spatial metric $\gamma_{ij} = \chi \tilde{\gamma}_{ij}$. The line element in this formulation is usually written as

$$ds^2 = -\alpha^2 dt^2 + \chi^{-1} \gamma_{ij} (dx^i + \beta^i dt)(dx^j + \beta^j dt), \quad (13)$$

where α is the lapse and β^r is the shift, the gauge quantities that are evolved besides χ and γ_{ij} . The conformal extrinsic curvature tensor \bar{K}_{ij} is divided into its trace and trace-free parts,

$$A_{ij} = \chi \bar{K}_{ij} - \frac{1}{3} \gamma_{ij} \bar{K}, \quad (14)$$

where $\bar{K} = \tilde{\gamma}^{ij} \bar{K}_{ij}$. Instead of using \bar{K} , we will instead define this new variable K ,

$$K = \bar{K} - 2\Theta, \quad (15)$$

where Θ is a quantity belonging to the Z4 part of the formulation. Lastly,

$$\Lambda^i = \Delta \Gamma^i + 2\gamma^{ij} Z_j, \quad (16)$$

with $\Delta \Gamma^i = \Gamma^i - \hat{\Gamma}^i$ and $\Gamma^i = \gamma^{jk} \Gamma_{jk}^i$. $\hat{\Gamma}_{jk}^i$ is the connection coming from a time-independent spatial metric $\hat{\gamma}_{ij}$ of our choosing, which we set to the flat spatial metric. From the Einstein equations, we evolve γ_{ij} , χ , α , β^i , A_{ij} , \bar{K} , Λ^i and $\hat{\Theta}$. The physical \bar{K} and $\hat{\Theta}$ are related to their conformal counterparts as,

$$\tilde{K} = \Omega K - \frac{3\beta^i \partial_i \Omega}{\alpha}, \quad \tilde{\Theta} = \Omega \Theta. \quad (17)$$

In spherical symmetry only the scalar quantities and the radial components of vectors and tensors are evolved.

C. Charged Scalar Field

Adapting to the notation mentioned in the previous section, the physical scalar field now appears with a tilde on top, $\tilde{\phi}$. It is useful to define the rescaled scalar field $\bar{\phi}$ from the physical one $\tilde{\phi}$:

$$\bar{\phi} = \frac{\tilde{\phi}}{\Omega}, \quad (18)$$

From this, the definitions for the real and imaginary parts of the scalar field are,

$$\bar{\phi} = \bar{c}_\phi + i\bar{d}_\phi, \quad \bar{c}_\phi, \bar{d}_\phi \in \mathbb{R}, \quad (19)$$

such that the modulus of the scalar field is defined as

$$|\bar{\phi}| = \sqrt{\bar{c}_\phi^2 + \bar{d}_\phi^2}. \quad (20)$$

The corresponding time derivatives of both parts of the scalar field are also defined as,

$$\bar{c}_\Pi = \partial_t \bar{c}_\phi, \quad \bar{d}_\Pi = \partial_t \bar{d}_\phi. \quad (21)$$

III. INITIAL DATA

As indicated in [36], the simplest condition to initially satisfy the momentum constraint, having a scalar field perturbation in \bar{c}_ϕ , is

$$\bar{c}_\Pi = \beta^r \left(\bar{c}'_\phi + \bar{c}_\phi \frac{\Omega'}{\Omega} \right), \quad (22)$$

where β^r is the radial component of the shift and the prime indicates a spatial derivative ($\phi' = \partial_r \phi$). However, when performing simulations with these initial data, it was hard to reach the tail regime with the expected exponent. Therefore, we followed Ref. [31] and changed the initial data such that we had the freedom to choose a more ingoing or outgoing pulse, but still solving the constraints initially. To do so, we add a new variable ψ_A , such that the initial value for A_{rr} changes to,

$$A_{rr0} \psi^{-6} \rightarrow (A_{rr0} + \psi_A) \psi^{-6}, \quad (23)$$

where ψ is the variable that we use to solve the Hamiltonian constraint for and ψ_A the variable that we solve the momentum constraint for. The substitution performed for χ is

$$\chi \rightarrow \chi_0 \psi^{-4}. \quad (24)$$

Additionally, in Ref. [31] a helper variable is defined,

$$\check{\Pi} = \frac{\gamma_{\theta\theta} \sqrt{\gamma_{rr}}}{\alpha \chi^{3/2}} \left(\dot{\bar{\Phi}} - \beta^r \check{\Phi}' \right), \quad (25)$$

where the dot denotes a time derivative ($\dot{\phi} = \partial_t \phi$). Expressing (25) in our variables yields

$$\check{\check{c}}_\Pi = \frac{\gamma_{\theta\theta} \sqrt{\gamma_{rr}}}{\alpha \chi^{3/2}} \left(\bar{c}_\Pi - \beta^r \left(\bar{c}'_\phi + \bar{c}_\phi \frac{\Omega'}{\Omega} \right) \right), \quad (26)$$

where \check{c}_{Π} is our new helper variable. As initial data for it, we choose,

$$\check{c}_{\Pi 0} = \sigma \frac{\gamma_{\theta\theta 0} \sqrt{\gamma_{rr 0}}}{\alpha_0 \chi_0^{3/2}} \beta^r \left(\check{c}'_{\phi 0} + \bar{c}_{\phi 0} \frac{\Omega'}{\Omega} \right),$$

with σ a real number usually taken to be ± 1 . Reverting back the changes from the previous equations, we get that the initial data for $\bar{c}_{\Pi 0}$ is

$$\bar{c}_{\Pi 0} = \beta^r \left(\check{c}'_{\phi} + \bar{c}_{\phi} \frac{\Omega'}{\Omega} \right) \left(1 + \frac{\sigma}{\psi^6} \right). \quad (27)$$

The difference between the above and (22) is the last factor involving ψ and σ . The sign of σ will imply a mostly ingoing or outgoing, depending on whether it takes the value of -1 or 1. In this paper, we will use $\sigma = 0$ for a longer QNM ringing (which is equivalent to (22)), and $\sigma = -1$ for the tail regime analysis. The initial data for the rest of the variables is available in [36].

Going back to (23), to solve the momentum constraint ψ_A has to fulfill the following differential equation

$$\begin{aligned} \psi'_A = & -\frac{8\pi\bar{\Omega}^3\check{c}_0(\check{c}'_{\phi}\Omega + \bar{c}_{\phi}\Omega')}{\Omega^3} \\ & -\psi_A \left(\frac{3}{r} \left[\left(1 - \frac{2M\bar{\Omega}}{r} + \frac{Q^2\bar{\Omega}^2}{r^2} \right) + \right. \right. \\ & \left. \left. + \left(\frac{K_{\text{CMC}}r}{3\bar{\Omega}} + \frac{C_{\text{CMC}}\bar{\Omega}^3}{r^2} \right)^2 \right]^{1/2} + \frac{\Omega'}{\Omega} \right), \end{aligned} \quad (28)$$

with C_{CMC} being a constant. Note that this equation is independent of ψ . We show how the solution looks for several values of the charge in Fig. 1, keeping $M = 1$ and $K_{\text{CMC}} = -1$. C_{CMC} is chosen to be the critical value corresponding to the values of M , K_{CMC} and Q that gives us trumpet initial data – see subsection 3.3.2 in [31] for more details. Furthermore, we chose the scalar field perturbation on \bar{c}_{ϕ} to be Gaussian-like, centered at $\mu = 0.5$, with $\sigma = 0.1$ and the amplitude A to be 0.001:

$$\bar{c}_{\phi 0} = r^2 A \exp \left(-\frac{(r^2 - \mu^2)^2}{\sigma^4} \right). \quad (29)$$

The equation for ψ , when solving the Hamiltonian constraint only for a perturbation in \bar{c}_{Π} is given by

$$\begin{aligned} \psi'' = & -\frac{3C_{\text{CMC}}^2\bar{\Omega}^4}{4r^6\psi^7} - \frac{K_{\text{CMC}}^2\psi}{12\bar{\Omega}^2} + \frac{Q^2\bar{\Omega}^2\psi}{4r^4} \\ & + \frac{3C_{\text{CMC}}^2\bar{\Omega}^4\psi}{4r^6} + \frac{K_{\text{CMC}}^2\psi^5}{12\bar{\Omega}^2} - \frac{\pi\bar{\Omega}^4\check{c}_0^2}{\psi^7\Omega^4} \\ & + \frac{C_{\text{CMC}}\bar{\Omega}\psi_A\Omega}{4r^3\psi^7} - \frac{3\psi_A^2\Omega^2}{16\bar{\Omega}^2\psi^7} - \pi\psi\Omega^2(\check{c}'_{\phi})^2 - \frac{\psi'}{r} \\ & - \frac{\psi'}{3r^3\bar{\Omega}} \left(K_{\text{CMC}}^2r^6 + 9r^4\bar{\Omega}^2 + 9Q^2r^2\bar{\Omega}^4 \right. \\ & \left. + 6(C_{\text{CMC}}K_{\text{CMC}} - 3M)r^3\bar{\Omega}^3 + 9C_{\text{CMC}}^2\bar{\Omega}^6 \right)^{1/2} \\ & - 2\pi\bar{c}_{\phi}\psi\Omega\check{c}'_{\phi}\Omega' - \pi\check{c}_{\phi}^2\psi\Omega'^2. \end{aligned} \quad (30)$$

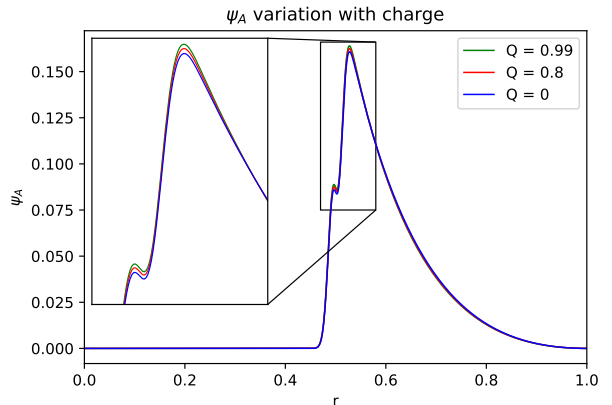


FIG. 1: Numerical solution for ψ_A solving (28) for several values of the black hole's charge. We show a zoom-in on the region where it is easier to see the effect of the charge on ψ_A . M is set to 1 and K_{CMC} to -1.

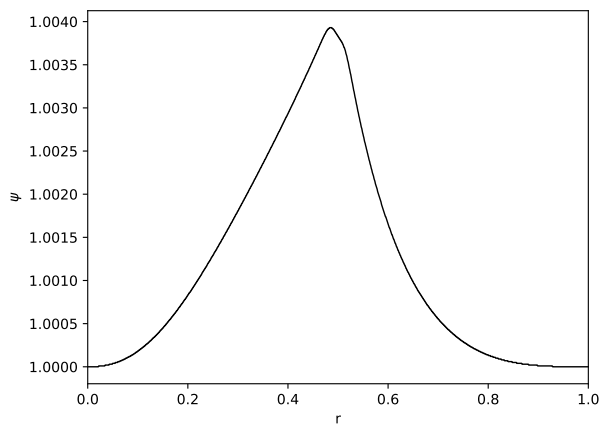


FIG. 2: Integrating (30) to get the numerical solution for ψ , assuming $Q = 0$. For other values of charge, the result is similar.

The result from integrating (30), including the previously obtained numerical solution for ψ_A , is shown in Fig. 2, assuming $Q = 0$. For other values of the charge, the end result is visually indistinguishable.

IV. QUASINORMAL MODES

It is easiest to observe the QNM ringing when the charges of the black hole and the scalar field are set to 0, which corresponds to the usual Klein-Gordon field in Schwarzschild spacetime. Recall that in this section we use (22), as done in [31, 36]. We have further set the following parameters for the real part of the scalar field perturbation (29): $A = 0.0005$, $\mu = 0.4$ and $\sigma = 0.05$. The QNM ringing is shown in Fig. 3, together with the Cowling approximation [40, 41], which corresponds to fixing the background and not evolve the Einstein equations. We also show the same setup for a charged black

hole with $Q = 0.5$ and setting the scalar field's charge to $q = 1.0$.

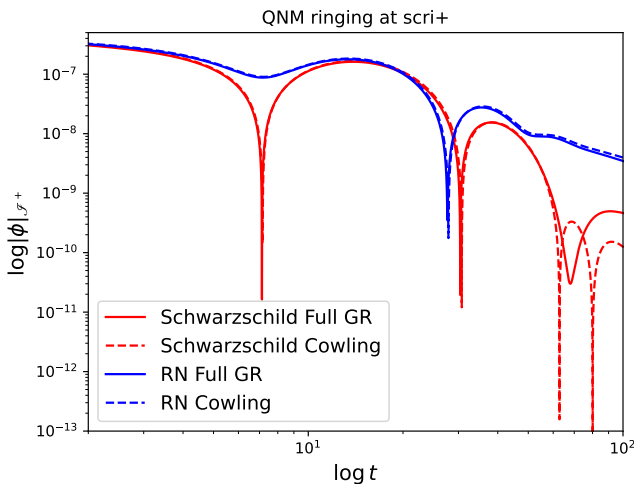


FIG. 3: Comparison of quasinormal mode ringing of a scalar field perturbation of Schwarzschild and RN spacetimes (called *Full GR* in the plot). We also show the Cowling approximations, i.e., not evolving the background (called *Cowling* in the plot). We plot this and the following time-dependent graphs in terms of the logarithm of the unrescaled code time t instead of $\log(t/M)$, as the total mass of the system changes depending on the contribution of the scalar field that falls into the black hole.

Only in the Schwarzschild case were we able to fit the fundamental spherical mode, because the charged case does not show enough oscillations to be able to estimate their period. Following Refs. [3, 42], we assume the shape of the mode to be described by a damped oscillating exponential $e^{-i\omega t}$, with $\omega \approx 0.11 - 0.10i$ and show the fitting to the data from the simulation in Fig. 4. This coincides with the result obtained in [43].

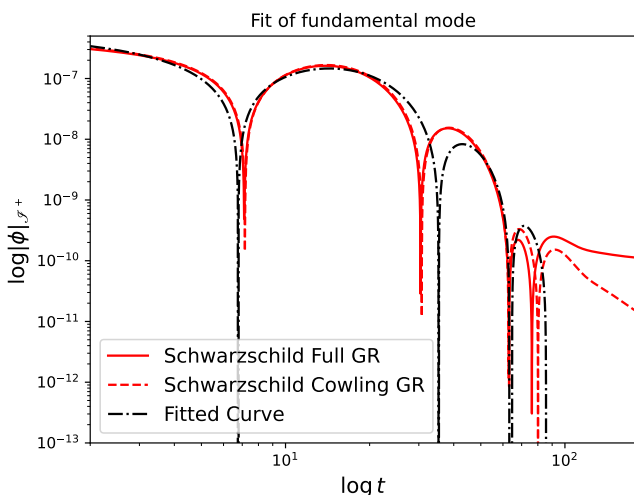


FIG. 4: Fitting the fundamental mode to the QNM ringing of the real scalar field, in a Schwarzschild spacetime.

For sufficiently strong electromagnetic coupling between both objects ($qQ > 0.001$), the amount of oscilla-

tions coming from the QNM ringing is indeed too small to do a reliable fit. We suspect that the cause of the almost absent ringing is that as soon as the imaginary part picks up on the initial real perturbation, both real and imaginary parts start to oscillate at a very precise frequency (this will be discussed in detail in section V), not allowing the overall amplitude of the scalar field to have the same behavior as it would in the purely real case.

V. LATE-TIME BEHAVIOR

To check the late-time behavior of the scalar field's perturbation of a RN black hole (after the QNM ringing), we now use the initial data for \bar{c}_{Π} in (27). The scalar field's charge is set to 1.0. Regarding the charge of the black hole Q , we have ran several simulations, each with a different value of Q , to see the effect of the parameter qQ [8, 9, 12] on the exponent of the power-law regarding the decay. The results are shown in Fig. 5. The relevant quantity to look at is the amplitude of the scalar field (20). For low values of qQ (i.e., the top left graph), both the real and imaginary parts enter a power-law decay, mostly dominated by the real part. However, as we increase qQ , the real and imaginary parts continue to oscillate one around the other, presumably due to the increased electric coupling between each other. Even during their oscillation, their amplitude decreases with a fixed power-law tail. Note also that the frequency of oscillation during the tail regime increases with qQ .

VI. TAIL REGIME

To better analyze the tail decays' exponents (3)-(4), we plot the following quantity,

$$\left. \frac{d \log |\phi|}{d \log t} \right|_{\text{late-time}} = \frac{d}{d \log t} \log (At^p) = p \quad (31)$$

where p is the exponent and A is the amplitude of the scalar field at the point it enters the tail regime. The exponent p attains in spherical symmetry, along a null hypersurface such as \mathcal{S}^+ and at timelike infinity, the following expressions [11]:

$$p_{\mathcal{S}^+} = \text{Re}(-\beta) - 1, \quad p_{i^+} = \text{Re}(-2\beta) + 2, \quad (32)$$

where $\text{Re}(\beta)$ means the real part of β . (3) also tells us that there is a limit to the real part of β , when $4(qQ)^2 > 1$, i.e., when $qQ > 1/2$ or $qQ < -1/2$. It is important to note that our simulations do not reach i^+ . They would if we were to leave the simulation to run for an infinite amount of time. However, it is expected that, as time increases, the decay of the scalar field at a given radius smaller than $r_{\mathcal{S}^+}$ will tend to the decay rate at i^+ . Therefore, from now on we compare the behavior of the scalar field at a given extraction radius of our choice with the decay rate p_{i^+} given by the expression in (32).

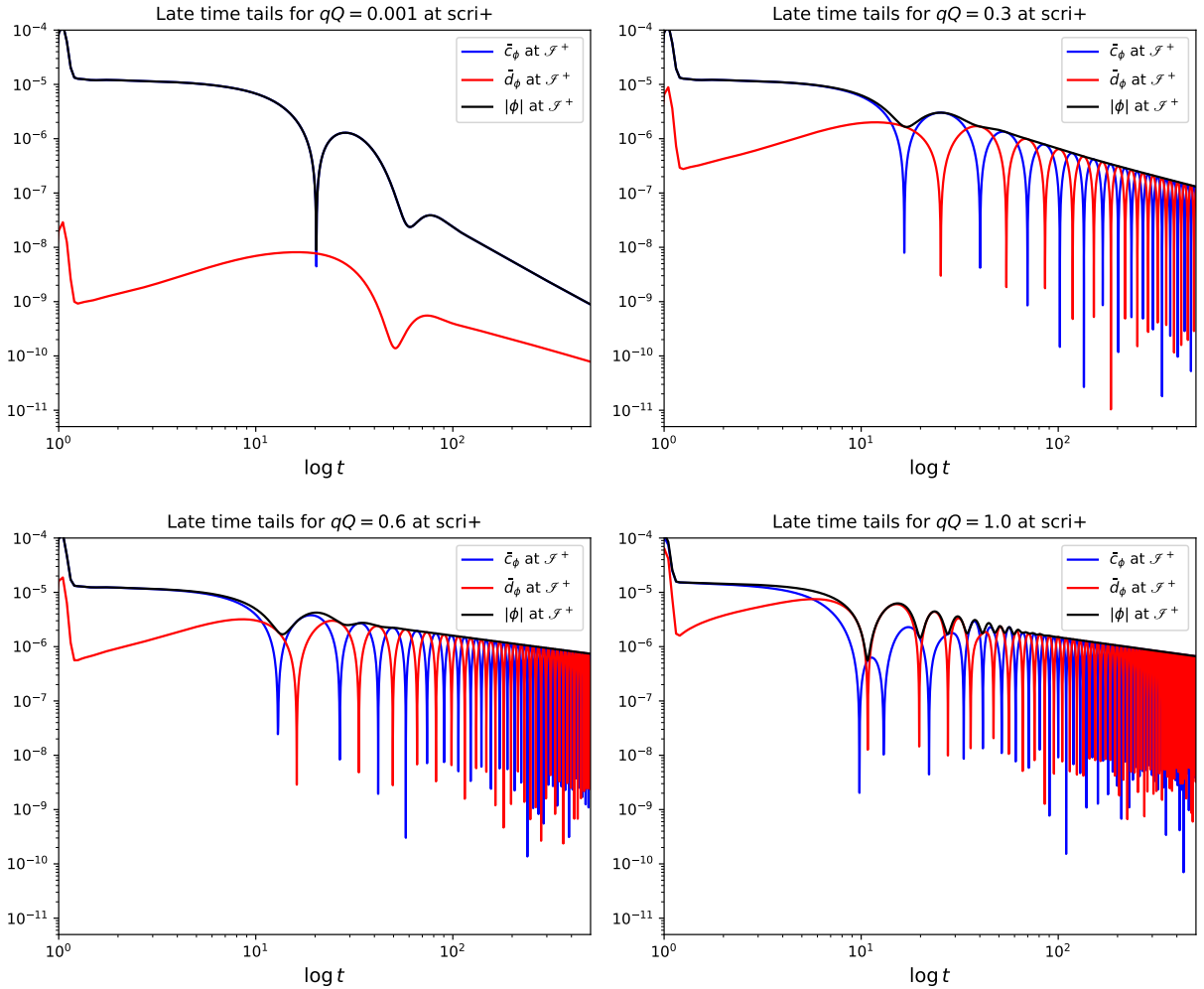


FIG. 5: Late-time tails at \mathcal{S}^+ for a charged scalar field in a charged background. The scalar field's charge is set to 1 and the black hole's charge is different in each plot (from top left to bottom right: 0.0001, 0.3, 0.6 and 1.0). The black line in all graphs corresponds to the amplitude of the scalar field (20). The mass of the black hole is set to 1, making the last graph correspond to an extreme RN black hole.

Plotting the data output from our simulation as in (31), we get Fig. 6.

For $qQ = 0.6$ and $qQ = 1.0$ both signals oscillate around $p = -0.5$ and $p = -1.0$ for \mathcal{S}^+ and $r \approx 0.75$, respectively, meaning that the maximum real part of β has been reached (check (32) and (3)). To understand better how the exponent changes, we considered more values of qQ . To get precise values of p , we did a linear regression on $d \log |\phi| / d \log t$ between $t = 100$ and $t = 150$ and the slope of each regression corresponds to the p of that same simulation. The results are plotted in Fig. 7, where they are compared to previous analytical results in the literature.

The most relevant conclusion here is that expressions (4) and (3) describe well how p changes with qQ , except for $qQ \ll 1$, where the better approximation is the same as in the uncharged case. There is a transition phase between both regimes, which indicates the change

from gravitational to electromagnetic effects. As far as we know, this is the first time a continued comparison has been shown of both regimes of the scalar field's tail decay. Although this effect has been addressed in the literature, there has not been a clear understanding of how this transition happens. It would be interesting to explore better how to construct a tail decay that is partially affected by the gravitational curvature and by the electromagnetic coupling.

We also wanted to see the effect of qQ in the oscillation frequency of the real and imaginary parts of the scalar field at \mathcal{S}^+ . For $qQ < 1/2$, (4) implies that the frequency should increase linearly with this charge parameter. For $qQ > 1/2$, we have to take into account the imaginary part that comes from β . To compare the analytical results with our simulation, we applied a Fourier transform to the real part (or equivalently to the imaginary part) of the scalar field during the tail regime. When plot-

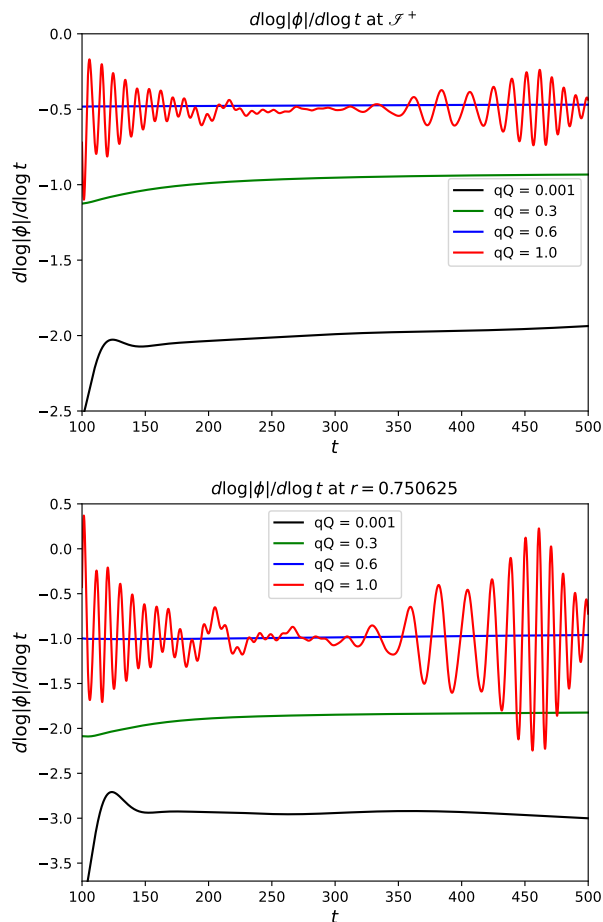


FIG. 6: Derivative of the log of the absolute value of the scalar field with respect to the log of time. This gives the time exponent for each value of the charge parameter Qq , top for \mathcal{S}^+ and bottom for $r \approx 0.75$.

ting our results against the prediction (4), there seemed to be an order of magnitude of difference, namely, that for $qQ < 1/2$, the frequencies coming from our simulation were exactly 10 times smaller. Therefore, in Fig. 8, we show the imaginary part of (4) divided by 10, the frequencies of the real part of the scalar field as qQ increases, and a blue line that corresponds to $\text{Frequency} = qQ/10$. This blue line is an empirical guess that suits better the data than the prediction. Thus, while for p the theoretical predictions were in agreement with our simulations, for the frequency analysis we see a clear divergence especially for $qQ > 1/2$.

VII. CONCLUSIONS

With this work, we took advantage of hyperboloidal slices to gain access to \mathcal{S}^+ efficiently to understand the behavior of a charged scalar field perturbation of a RN black hole. This allowed us to study the QNM ringing of the scalar field in Schwarzschild and RN spacetimes and found it only possible to fit the spherical fundamen-

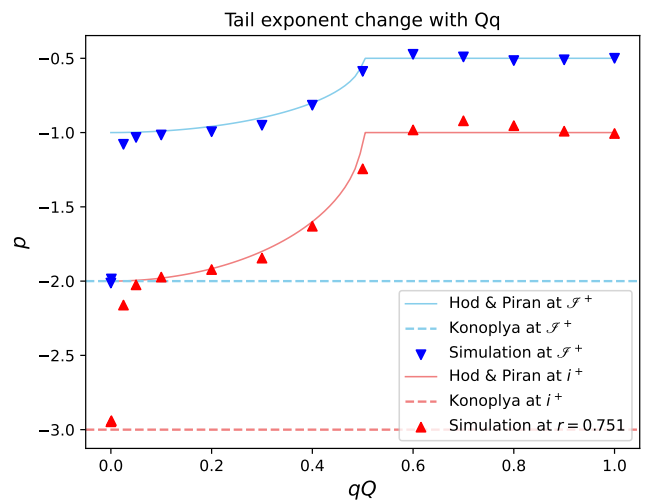


FIG. 7: Comparison of the results from our simulation (the triangles) with the analytical results coming from Konoplya and Zhidenko [12] and from Hod and Piran [9]. As was mentioned in the main body of the text, the red lines correspond to the expected decay of the scalar field at i^+ . The red points, however, correspond to the decay of the scalar field at a given radius $r \approx 0.75$ and at finite time, which is not i^+ . Nonetheless, as the simulation time increases, the decay we expect to see at $r < 1$ should approach asymptotically the one at i^+ .

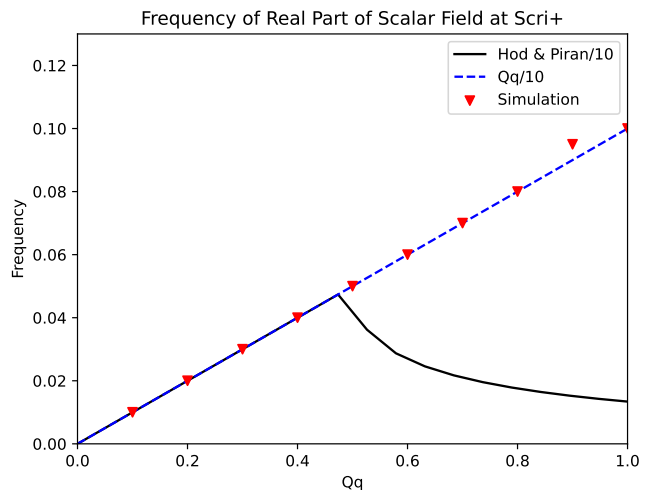


FIG. 8: Frequency comparison of the results from our simulation (the triangles) with one tenth of the analytical results coming from Hod and Piran [9], (4), (the black line). The blue line corresponds to the function $f = Qq/10$, an empirical guess that shows better agreement.

tal mode to the former case. The latter showed but one oscillation, making it difficult to construct a reliable fit. We propose that the reason for the almost complete absence of oscillations is due to the self interaction of the charged scalar field, which picks up as soon as the imaginary part is excited by the presence of the charged black hole. Regarding the tail regime, although our results agree very well with Ref. [11], there is a transition region where the decay is affected both by the black hole's cur-

vature and also by the electromagnetic coupling that to this day seems to have been unaddressed, to the best of our knowledge. The fact that this transition occurs around $Qq \sim 10^{-3}$, means that, contrary to the point-of-view that electrically charged black holes might be astrophysically irrelevant [44], even if a black hole has a very small amount of charge, it may have a noticeable impact on the late-time behavior of perturbations.

We also analysed the frequency of oscillation of the real and imaginary parts during the tail regime and found a linear correlation between Qq and the frequency with which they oscillate. For $Qq > 1/2$, the expected frequency seems to deviate from the analytical predictions in Ref. [11].

Natural extensions of this work will involve studying the decay tails that originate in a collapsing space-time [45] – for a sample simulation of charged collapse with our infrastructure see Ref. [36]. This will allow us to compare to prior results obtained at future null infinity [46]. The prospect of tuning the collapse towards the extremal case $Q = M$ [47] is especially exciting. Another option is to consider a scalar-field-dependent coupling with the Maxwell part such as Ref. [48] and study the behaviour of the resulting hairy black holes. Recent work [49] used hyperboloidal slices to study quasinormal modes of Boulware-Deser-Wheeler black holes in Einstein-Gauss-Bonnet gravity. Given the potential ill-posedness of the latter, attempting a full non-linear simulation of this setup is too risky at this stage, but could be an interesting research line to follow in the future.

Acknowledgements

The authors would like to thank Christian Peterson Bórquez for useful advice regarding the ringing of QNM in hyperboloidal slices and to Adrien Kuntz and Nicola Franchini for the help finding important references for this work. The acknowledgements extend naturally to Vitor Cardoso and again to Adrien for very useful comments on the manuscript.

AVV thanks the Fundação para a Ciência e Tecnologia (FCT), Portugal, for the financial support to the Center for Astrophysics and Gravitation (CENTRA/IST/ULisboa) through the Grant Project No. UIDB/00099/2020. This work was also supported by the Universitat de les Illes Balears (UIB); the Spanish Agencia Estatal de Investigación grants PID2022-138626NB-I00, RED2022-134204-E, RED2022-134411-T, funded by MICIU/AEI/10.13039/501100011033 and the ERDF/EU; and the Comunitat Autònoma de les Illes Balears through the Conselleria d'Educació i Universitats with funds from the European Union - NextGenerationEU/PRTR-C17.I1 (SINCO2022/6719) and from the European Union - European Regional Development Fund (ERDF) (SINCO2022/18146). JDA thanks Fundação para a Ciência e Tecnologia (FCT), Portugal, for the financial support through the Grant Project 2024.04456.CERN.

-
- [1] K. D. Kokkotas and B. G. Schmidt, *Living Rev. Rel.* **2**, 2 (1999), gr-qc/9909058.
- [2] R. A. Konoplya and A. Zhidenko, *Rev. Mod. Phys.* **83**, 793 (2011), 1102.4014.
- [3] E. Berti, V. Cardoso, and A. O. Starinets, *Classical and Quantum Gravity* **26**, 163001 (2009), ISSN 0264-9381, 1361-6382, arXiv:0905.2975 [gr-qc], URL <http://arxiv.org/abs/0905.2975>.
- [4] E. Berti et al. (2025), 2505.23895.
- [5] R. H. Price, *Nonspherical Perturbations of Relativistic Gravitational Collapse. I. Scalar and Gravitational Perturbations* | *Phys. Rev. D*, URL <https://journals.aps.org/prd/abstract/10.1103/PhysRevD.5.2419>.
- [6] C. Gundlach, R. Price, and J. Pullin, *Physical Review D* **49**, 883 (1994), ISSN 0556-2821, arXiv:gr-qc/9307009, URL <http://arxiv.org/abs/gr-qc/9307009>.
- [7] M. De Amicis et al. (2024), 2412.06887.
- [8] J. Bičák, *General Relativity and Gravitation* **3**, 331 (1972), ISSN 0001-7701, 1572-9532, URL <http://link.springer.com/10.1007/BF00759172>.
- [9] S. Hod and T. Piran, *Physical Review D* **58**, 024017 (1998), ISSN 0556-2821, 1089-4918, arXiv:gr-qc/9712041, URL <http://arxiv.org/abs/gr-qc/9712041>.
- [10] S. Hod and T. Piran, *Physical Review D* **58**, 024018 (1998), ISSN 0556-2821, 1089-4918, arXiv:gr-qc/9801001, URL <http://arxiv.org/abs/gr-qc/9801001>.
- [11] S. Hod and T. Piran, *Physical Review D* **58**, 024019 (1998), ISSN 0556-2821, 1089-4918, arXiv:gr-qc/9801060, URL <http://arxiv.org/abs/gr-qc/9801060>.
- [12] R. A. Konoplya and A. Zhidenko, *Physical Review D* **88**, 024054 (2013), publisher: American Physical Society, URL <https://link.aps.org/doi/10.1103/PhysRevD.88.024054>.
- [13] B. Camden, J. Frauendiener, J. Galinski, K. Pillay, C. Stevens, and S. Thwala, *Gen. Rel. Grav.* **57**, 64 (2025), 2503.17631.
- [14] J. Winicour, *Living Rev. Rel.* **15**, 2 (2012).
- [15] N. T. Bishop, R. Gomez, L. Lehner, and J. Winicour, *Phys.Rev.* **D54**, 6153 (1996).
- [16] N. W. Taylor, M. Boyle, C. Reisswig, M. A. Scheel, T. Chu, et al., *Phys.Rev.* **D88**, 124010 (2013), 1309.3605.
- [17] J. Moxon, M. A. Scheel, S. A. Teukolsky, N. Deppe, N. Fischer, F. Hébert, L. E. Kidder, and W. Throwe, *The SpECTRE Cauchy-characteristic evolution system for rapid, precise waveform extraction* (2021), arXiv:2110.08635 [gr-qc], URL <http://arxiv.org/abs/2110.08635>.
- [18] N. Bishop, R. Gomez, L. Lehner, and J. Winicour, *Cauchy-characteristic extraction in numerical relativity* (1997), arXiv:gr-qc/9705033, URL <http://arxiv.org/abs/gr-qc/9705033>.

- [19] S. Ma, J. Moxon, M. A. Scheel, K. C. Nelli, N. Deppe, M. S. Bonilla, L. E. Kidder, P. Kumar, G. Lovelace, W. Throwe, et al., *Fully relativistic three-dimensional Cauchy-characteristic matching* (2023), arXiv:2308.10361 [gr-qc], URL <http://arxiv.org/abs/2308.10361>.
- [20] S. Ma, M. A. Scheel, J. Moxon, K. C. Nelli, N. Deppe, L. E. Kidder, W. Throwe, and N. L. Vu (2024), 2412.06906.
- [21] R. Penrose, Phys. Rev. Lett. **10**, 66 (1963), URL <http://link.aps.org/doi/10.1103/PhysRevLett.10.66>.
- [22] H. Friedrich, Comm. Math. Phys. **91**, 445 (1983), URL <http://projecteuclid.org/euclid.cmp/1103940664>.
- [23] P. Hübner, Class.Quant.Grav. **16**, 2145 (1999), gr-qc/9804065.
- [24] J. Frauendiener, Phys.Rev. **D58**, 064002 (1998), gr-qc/9712050.
- [25] T. Nakamura, K. Oohara, and Y. Kojima, Prog. Theor. Phys. Suppl. **90**, 1 (1987).
- [26] M. Shibata and T. Nakamura, Phys. Rev. D **52**, 5428 (1995), URL <http://link.aps.org/doi/10.1103/PhysRevD.52.5428>.
- [27] T. W. Baumgarte and S. L. Shapiro, Phys.Rev. **D59**, 024007 (1999), gr-qc/9810065.
- [28] C. Bona, T. Ledvinka, C. Palenzuela, and M. Žáček, Physical Review D **67**, 104005 (2003), ISSN 0556-2821, 1089-4918, URL <https://link.aps.org/doi/10.1103/PhysRevD.67.104005>.
- [29] A. Zenginoglu, Class. Quantum Grav. **25**, 145002 (2008), ISSN 0264-9381, 1361-6382, arXiv:0712.4333 [gr-qc], URL <http://arxiv.org/abs/0712.4333>.
- [30] A. Vañó-Viñuales, S. Husa, and D. Hilditch, Class. Quant. Grav. **32**, 175010 (2015), 1412.3827.
- [31] A. Vañó-Viñuales, *Free evolution of the hyperboloidal initial value problem in spherical symmetry* (2015), arXiv:1512.00776 [gr-qc], URL <http://arxiv.org/abs/1512.00776>.
- [32] A. Vañó-Viñuales and S. Husa, Class. Quant. Grav. **35**, 045014 (2018), 1705.06298.
- [33] A. Vañó Viñuales, Front. Appl. Math. Stat., Sec. Statistical and Computational Physics **9** (2023), 2304.05384.
- [34] A. Vañó Viñuales, Class. Quant. Grav. **41**, 105003 (2024), 2311.04972, URL <https://dx.doi.org/10.1088/1361-6382/ad3aca>.
- [35] A. Vañó Viñuales and T. Valente, General Relativity and Gravitation **56** (2024), 2408.08952.
- [36] J. D. Álvarez and A. Vaño-Viñuales, *Free Hyperboloidal Evolution of the Einstein-Maxwell-Klein-Gordon System* (2025), arXiv:2505.17176 [gr-qc], URL <http://arxiv.org/abs/2505.17176>.
- [37] S. Aretakis, Communications in Mathematical Physics **307**, 17 (2011), ISSN 1432-0916, URL <https://doi.org/10.1007/s00220-011-1254-5>.
- [38] J. D. López and M. Alcubierre, *Charged boson stars revisited* (2023), arXiv:2303.04066 [gr-qc], URL <http://arxiv.org/abs/2303.04066>.
- [39] V. Jaramillo, D. Núñez, M. Ruiz, and M. Zilhão, *Full 3D nonlinear dynamics of charged and magnetized boson stars* (2024), arXiv:2411.07284 [gr-qc], URL <http://arxiv.org/abs/2411.07284>.
- [40] T. G. Cowling, Monthly Notices of the Royal Astronomical Society **101**, 367 (1941), ISSN 0035-8711, URL <https://doi.org/10.1093/mnras/101.8.367>.
- [41] A. Maniopoulos and N. Andersson, Monthly Notices of the Royal Astronomical Society **351**, 1349 (2004), ISSN 0035-8711, URL <https://doi.org/10.1111/j.1365-2966.2004.07872.x>.
- [42] C. Peterson, S. Gautam, A. Vañó-Viñuales, and D. Hilditch, *Spherical Evolution of the Generalized Harmonic Gauge Formulation of General Relativity on Compactified Hyperboloidal Slices* (2024), arXiv:2409.02994 [gr-qc], URL <http://arxiv.org/abs/2409.02994>.
- [43] C. Peterson and D. Hilditch (2025), 2506.03078.
- [44] S. L. Shapiro and S. A. Teukolsky, *Black holes, white dwarfs and neutron stars. The physics of compact objects* (1983), publication Title: A Wiley-Interscience Publication ADS Bibcode: 1983bhwd.book.....S, URL <https://ui.adsabs.harvard.edu/abs/1983bhwd.book.....S>.
- [45] C. Gundlach, R. H. Price, and J. Pullin, Phys. Rev. D **49**, 890 (1994), gr-qc/9307010.
- [46] M. Purrer, S. Husa, and P. C. Aichelburg, Phys. Rev. D **71**, 104005 (2005), gr-qc/0411078.
- [47] C. Kehle and R. Unger (2024), 2402.10190.
- [48] H. Guo, W.-L. Qian, and B. Wang (2025), 2506.02445.
- [49] L.-M. Cao, L.-B. Wu, and Y.-S. Zhou (2024), 2412.21092.